Bio-Inspired Micro Robots Swimming in Channels

Fatma Zeynep Temel, Onder Erin, Ahmet Fatih Tabak and Serhat Yesilyurt[1]
Faculty of Engineering and Natural Sciences Mechatronics Department
Sabanci University
Istanbul, Turkey
[1]syesilyurt@sabanciuniv.edu

***Abstract*—Swimming micro robots that mimic micro organisms have a huge potential in biomedical applications such as opening clogged hard-to-reach arteries, targeted drug delivery and diagnostic operations. Typically, a micro swimmer that consists of a magnetic bead as its body, which is attached to a rigid helical tail, is actuated by a rotating external magnetic field and moved forward in the direction of the rotation in fluids. Understanding of hydrodynamic effects has utmost importance for modeling and prediction of the trajectory of the robot. In this work, a computational fluid dynamics (CFD) model is presented for the mm-long swimmer with the helical tail; the swimmer is used in our previous experiments on the effect of the confinement of the robot in a liquid filled channel. Forward velocity, fluid forces and torques on the micro swimmer are studied with respect to robot's radial position in the channel and the number of waves on the helical tail. Forward velocities from the CFD model for the robots swimming near the wall agree reasonably well with experimental measurements.**

I. INTRODUCTION

Swimming micro robots have great potential as tools that can promote minimally invasive surgery and perform several medical tasks, such as tissue repair and surveillance [1]. Recently, several experiments demonstrated that propulsion of untethered micro robots can be achieved with bio-inspired flagellar mechanisms such as rotation of helical rods or propagation of planar waves on flexible filaments [2, 3, 4]. Bacteria, such as *Escherichia coli,* propel themselves with the rotation of their helical flagella actuated by molecular motors; however, due to challenges of micro manufacturing and lack of space on the robots, actuation of artificial micro swimmers is controlled by means of an external magnetic field.

Studies in literature show that the velocity of natural micro organisms depends on not only the shape and size of the body, but also the rotation frequency, wavelength and amplitude of the flagellar motion [5, 6, 7]. Recently, Zhang *et al.* [3] manufactured artificial bacterial flagella from GaAs, having dimensions of 1.8μm in width, 30μm in length, and 200nm in thickness, which is attached to a soft magnetic head. Then the authors [3] applied a rotating magnetic field in the direction of the helical axis, and pointed out that resultant linear swimming velocity of the micro swimmer is affected by the size of the head and the strength of the magnetic field [3]. In another experimental study reported by Ghosh and Fischer [4], chiral colloidal propellers with dimensions of 200-300 nm width and 1-2μm length are made of ferromagnetic material deposited on silicon dioxide and navigated controllably with an external magnetic field in water with micrometer-level precision [4].

Hydrodynamic modeling of natural micro swimmers using helical wave propulsion and swimming in a pool or near solid boundaries has been an interest for over decades. Gray and Hancock presented the resistive force theory for the resultant propulsion and drag force calculation, from the integration of local forces in the normal and tangential directions that are proportional to the velocity components in that direction [8]. Sir James Lighthill proposed a line distribution of stokeslets on slender bodies and obtained resistive force coefficients for rotating rigid helical tails [9]. A broad review of propulsion mechanisms and parameters of micro organisms and theoretical models of micro propulsive effects are presented by Brennen and Winet [10]. Lauga *et al.* [11] studied the hydrodynamic behavior of *Escherichia coli* moving near plane boundaries based on drag coefficients presented by Katz *et al.* [12] accompanied with comparison on experimental and numerical results. Based on the Stokes-flow approach, Felderhof [13] discussed the velocity solutions to an infinite length helical filament without a payload. Lauga and Powers [14] presented a comprehensive review and discussion on hydrodynamic interactions of natural and artificial swimmers among themselves and with and nearby stationary boundaries.

In channel behavior of micro robots is important due to its relevance to *in vivo* applications. Recently we conducted a number of experiments with magnetically actuated in-channel swimming robots with $Nd_{12}Fe_{14}B$ bodies, a few hundred microns in diameter, and mm-long rigid helical tails, and demonstrated that the proportional relationship between the time-averaged swimming velocity and the frequency of the rotating magnetic field holds up to a step-out frequency which is dictated by the strength of the magnetic field and the size of the magnetic head [15] in channels as well and similarly to the results reported earlier in literature [3, 4]. The relation between the wave geometry and swimming velocities are presented in [16] via autonomous robots undergoing swimming

motion confined to oil-filled cylindrical channels of 3.6 cm in diameter.

Thorough understanding of the induced flow and hydrodynamic interactions of swimming micro robots with channel boundaries inside fluid-filled channels is required for controlled-navigation of micro robots inside bodily channels such as spinal cord or arteries. CFD is a useful tool that gives pointwise velocity distribution in the flow and the complete stress tensor on the boundaries, which are difficult to obtain directly by means of experiments. In this work, we present a three-dimensional CFD-model for the flow inside channels due to the motion of swimmers with helical tails governed by the Stokes flow, which is valid for low Reynolds number regime valid for small length scales. Effects of number of waves of the helical tail and proximity to the channel boundary on the speed, efficiency, and magnitude of forces and torques on the swimmer are analyzed by means of a number of CFD-simulation experiments. Moreover, simulation results are validated with the results obtained from our previous experiments.

II. METHODOLOGY

A. *Experimental Setup*

Micro robot used in the experiments consists of a magnetic head and a helical tail made of a copper wire of diameter 110 µm. In order to have high magnetization values in small volumes, lumps of $Nd_{12}Fe_{14}B$ that measure 150µm × 160µm × 170µm is used as the body of the swimmer. The non-magnetic wire with diameter of 110µm is deformed simply by coiling it up on another wire of diameter 360µm in order to obtain the helical-form tail (Fig.1). Wavelength, i.e. the distance between the helical turns, is measured as 520µm for four full waves on the tail. The helical tail is attached to the magnetic head with a strong adhesive and the robot is placed inside a glycerol filled glass channel having an inner diameter of 1mm. The density and viscosity of glycerol are measured as $\rho = 1000$ kg-m^{-3} and $\mu = 0.1$Pa-s, respectively.

Use of orthogonal Helmholtz coil pairs to obtain rotating magnetic field is a common in literature [3]. As in our previous experiments [15, 18], two orthogonal non-identical Helmholtz coil pairs are used to obtain spatially-uniform magnetic field (Fig.2) in a workspace of about 1 cm^3. The magnetic head rotates with the applied magnetic field as long as the resultant magnetic torque overcomes the viscous resistance of the fluid acting on the robot inside the glycerol filled channel. The necessary torque needed to rotate the micro swimmer is calculated from the cross product of the magnetic dipole moment, **m**, of the magnetic head of the robot with the magnetic induction, **B**, of the field generated by the coils [19]

$$\tau_{\mathrm{M}} = \mathbf{m} \times \mathbf{B} = \mu_0 \mathbf{m} \times \mathbf{H} \qquad (1)$$

where μ_0 is permittivity of the free space and **H** is magnetic field vector. Magnetic dipole moment is calculated by the magnetization of the material, **M**, and the volume of the particle, ϑ :

$$\mathbf{m} = \mathbf{M}\vartheta \qquad (2)$$

Thus from (1) and (2) we have the magnetic torque, which reads:

$$\tau_{\mathrm{M}} = \mu_0 \vartheta M H \sin\theta \qquad (3)$$

where H is the strength of the magnetic field and θ is the angle between **B** and **m** [19].

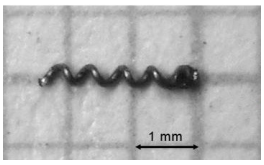

Figure 1. Micro robot used in the experiments.

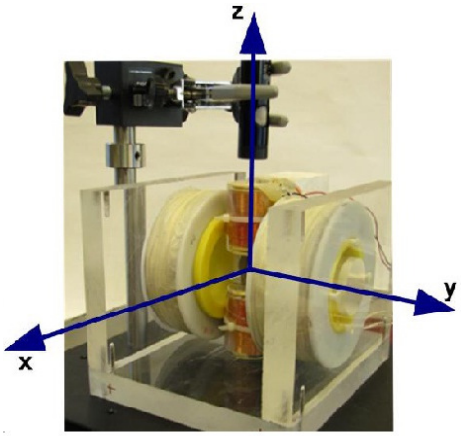

Figure 2. Experimental setup consists of two Helmholts coil pairs and the glass tube placed along **z-**axis of the setup [15].

The alternating current applied to Helmholtz coils in order to obtain a uniform rotating magnetic field is generated by via Maxon ADS_E 50/5 motor drives (Fig. 3a), which are connected to NI DAQ hardware. The magnitude and frequency of current are adjusted in LabView environment (Fig 3b and c). Swimming of micro robot is observed with TIMM-400 S/W v. 0.1-100 USB microscope having a resolution of 720 × 576 pixels with 30 frames per second recording rate. Average velocities of robots are calculated from the frames captured by the video camera.

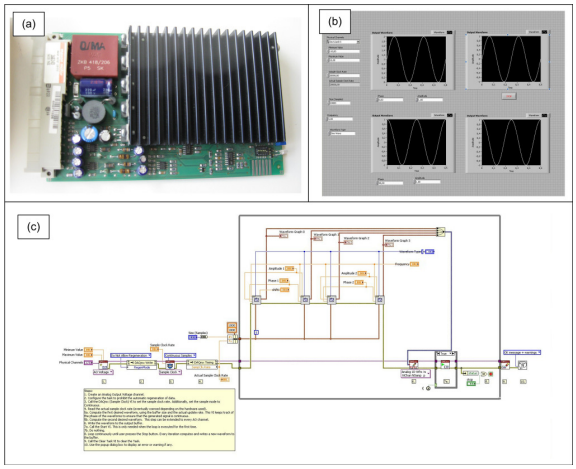

Figure 3. Each Helmholtz coil that constitutes the experimental setup is actuated by a Maxon ADS_E 50/5 Servoamplifier (a) which is controlles by NI LabView software: user interface (b) and block diagram(c).

B. CFD Modeling

Geometry of the micro swimmer in the CFD model is kept the same as the one used in the experiments. The body of the robot is assumed to be a perfect sphere and the helical tail is attached to it without any gap or mounting component. The spherical head has a diameter of D_h=360μm and the tail has a diameter of D_{wire}=110μm and has a length L_{tail} = 2.09mm axially (see Fig. 4). Due to high viscosity of the fluid inside the channel, the simulated length is set to L_{ch}=7.2 mm in order to reduce the computational requirements. Dissipative effects ensure the extent of the induced flow field to remain within the close proximity of the robot. The channel is filled with glycerol with a viscosity of μ = 0.1Pa-s, and density of ρ = 1000 kg-m^{-3} in simulations, the same as in the experiments. Diameter of the spherical head is assumed to be the reference length scale, which is used as the base value to scale other geometric dimensions in the CFD model.

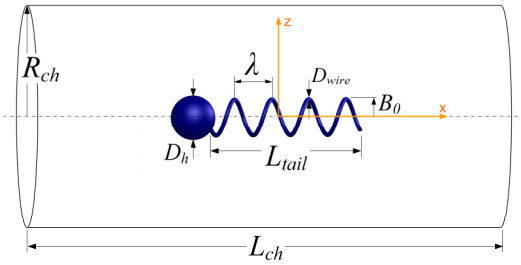

Figure 4. Parameters of the micro robot used in the experiments and modeled for CFD simulations.

The three-dimensional flow inside the channel is governed by incompressible Stokes equations subject to continuity. The inertial forces are negligible for low Reynolds numbers, thus the governing equations of the flow are:

$$0 = -\nabla P + \frac{1}{\mathrm{Re}_f}\nabla^2\mathbf{U} \qquad \textbf{in} \qquad \Omega(t) \tag{1}$$

$$\nabla \cdot \mathbf{U} = 0 \tag{2}$$

where P is pressure, $\mathbf{U}$ is the velocity vector, and Re_f is the frequency Reynolds number which is calculated as follows:

$$\mathrm{Re}_f = \frac{\rho D_h^2 f}{\mu} \tag{3}$$

where ρ and μ are the density and viscosity of the fluid, D_h is the diameter of the spherical head, and f denotes the frequency of swimmer rotations.

No-slip conditions are applied on channel walls including channel inlet and outlet forming a closed fluidic medium where the flow is initially at rest. Forward motion and rotation of the swimmer are defined as the velocity boundary conditions on the swimmer. The force free swimming condition is described in governing equations as a constraint equation:

$$F_x = \int_{S_{sw}} \sigma_{xj} d\mathbf{S}_j = 0, \tag{4}$$

where F_x is the total force on the swimmer in the **x**-direction, $d\mathbf{S}_j$ is the differential element at the surface that points in the jth direction, S_{sw} is the whole surface of the swimmer, and σ_{xj} is the stress tensor components in the **x**-direction, which is given by

$$\sigma_{xj} = -P\delta_{xj} + \mu\left(\frac{\partial u}{\partial x_j} + \frac{\partial u_j}{\partial x}\right) \tag{5}$$

where δ_{xj} Kronecker's delta, x_j={x,y,z} and u_j = {u,v,w}.

CFD simulations are carried out by COMSOL Multiphysics, which is a well-documented commercial finite element package [17]. The finite element model consists of approximately 150000 tetrahedral elements and 650000 degrees of freedom. It takes at least two hours to complete period on a dual six-core workstation operating at 3.2 GHz and with 96 GB RAM.

III. Results

Experiments are conducted for different frequency values changing between 5Hz and 50Hz. Micro robot is placed inside the glycerol-filled glass channel which is positioned along the **x**-axis of the experimental setup (see Fig. 2). With respect to the applied magnetic torque, swimming speed of micro swimmer has a linear relationship with the rotational frequency up to the step-out frequency (Fig. 5). After the step-out frequency, since the micro robot loses its sync with rotational magnetic field, the velocity reduces nonlinearly as the frequency increases. Magnetic field strength is measured as 7.41mT. Higher magnetic field strengths results with higher step-out frequency values [15]. Position and orientation of the micro robot inside the channel is not stable; according to the applied magnetic torque and rotational frequency, micro robot either swims at the center or near the wall of the channel (Fig 6). Calculated Reynolds number for the micro robot rotating at 10Hz is equal to 0.01296 which is far below 1 justifying the Stokes flow approach.

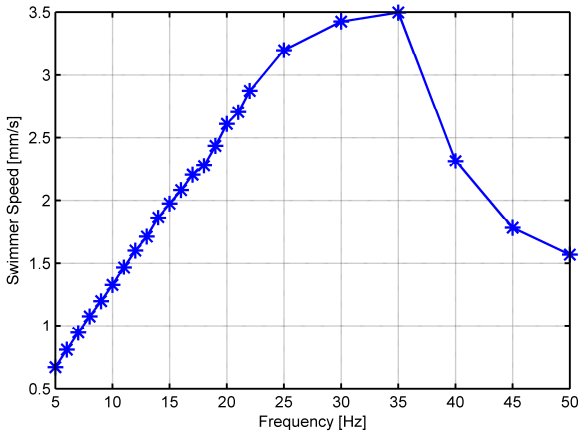

Figure 5. Swimming speed of micro robot inside channel with respect to rotational frequency.

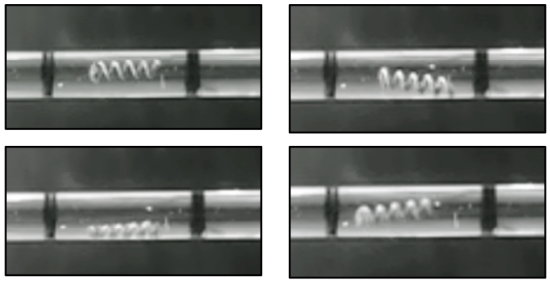

Figure 6. Different positions of micro robot inside glycerol-filled glass channel of 1mm-inner-diameter.

CFD-model simulations are carried out for angular positions of the robot ranging from 0 to 360 degrees, with nine different radial position values spaced between 0 and 0.30mm, and with total number of waves on the helical tail for N_λ = {2,3,4}. All lateral translation and rotations are restricted and the micro robot is free to translate and rotate along the **x**-axis.

Effects of number of waves and radial position of the micro robot on the time-averaged swimming velocity were studied in detail. Velocities were calculated by averaging out the simulation results for one complete turn of the micro swimmer. According to simulation results, instantaneous forward velocity of the micro swimmer with two full waves (max. 1.58mm/s) is bigger than the one with three full waves (max. 1.42mm/s) and the slowest one is the micro swimmer whose number of full waves on its helical tail is four (max. 1.19mm/s) (see Fig. 7). Furthermore, maximum forward velocity is reached when radial position of the robot is around 0.3 mm, which agrees with the theoretical results of Happel and Brenner [20] indicating that minimum drag force acting on a sphere in a fluid filled cylindrical channel occurs at 0.6-channel-radius away from the axis of the channel. The minimum forward velocity is observed when the swimmer is at the center. A nonlinear variation is observed in the forward velocity with respect to the radial position of the robot between the center of the channel and position where the maximum velocity is obtained. After that point on, as the distance between micro robots and the cylindrical channel wall decreases, velocity of the swimmers slightly reduces. Previous studies of Lauga *et al.* [11], which mainly focused on swimming near planar walls, demonstrated a similar drop in the speed of micro swimmers closer to the boundary. According to the experimental results, when micro robot is rotating with 10Hz, which is the case for the simulations as well, it travels with the velocity of 1.323mm/s. Simulation results confirms that micro robot is not swimming at the center but near the wall, since the maximum velocity of the micro robot with four full waves on the helical tail is obtained from the simulations as 1.19mm/s.

The net force on the swimmer in the **x**-direction is equal to zero as a result of the free swimming condition given by (4). In simulations, the swimmer is concentrically aligned with the symmetry axis of the channel, mean values of **y-** and **z-**forces acting on it are found to be zero due to symmetry, and as the swimmer is placed closer to the cylindrical channel wall, magnitudes of the **y-** and **z-**forces increase (see Fig. 8 and Fig.9). Positive **y**-force, which is the traction force due to the rotation of the swimmer, indicates that the swimmer is pushed to its starboard. The increase in the traction force is observed as the number of waves on the tail increases. The traction force first increases linearly with the radial position, then sharply as micro robot is placed further towards the channel wall.

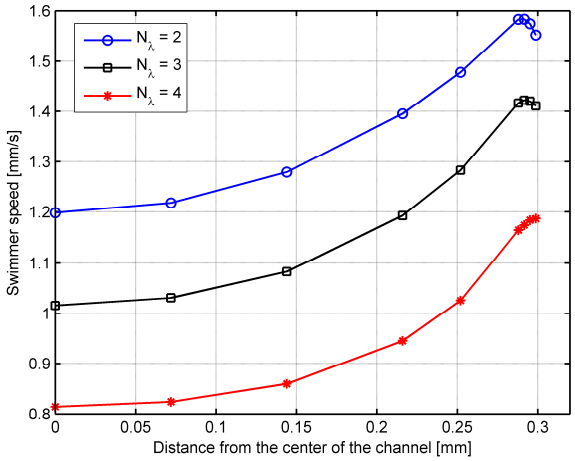

Figure 7. Forward velocities of the swimmers with respect to the distance from the center line of the channel for N_λ=2 (solid lines with circles), N_λ=3 (dashed line with circles), and N_λ=4 (dash-dotted line with '*'s).

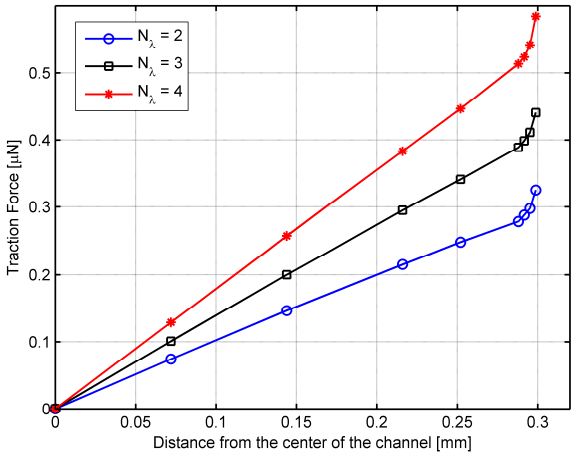

Figure 8. Traction forces acting on the swimmers with respect to the distance from the center line of the channel for N_λ=2 (solid lines with circles), N_λ=3 (dashed line with circles), and N_λ=4 (dash-dotted line with '*'s).

Resultant negative **z**-force is not as much effective as the traction force and indicates that the swimmer is pushed towards the channel wall with an increasing magnitude as the robot is placed further near the wall (Fig. 9) similarly to the "trapping" of the bacteria near walls as reported in literature [11]. Independent from the number of waves on the helical tail, the **z**-force shows the same behavior for all wavelengths.

The net torque in the **x**-direction is equal to the applied external magnetic torque and always attains its largest value for the micro robot with four waves on the helical tail. The minimum **x**-torque values are calculated at the point; where micro robot is at the centers; as 0.35 nN-m for N_λ=2, 0.39 nN-m for N_λ=3, and 0.43 nN-m for N_λ=4 (see Fig. 10). The magnitude of the **x**-torque increases nonlinearly and particularly rapidly

when the micro swimmer is placed in the vicinity of the channel wall. During experiments, it is also observed that, when swimmer approaches to the channel wall, the intensity of the magnetic field had to be increases to make sure the swimmer does not get into the step-out regime.

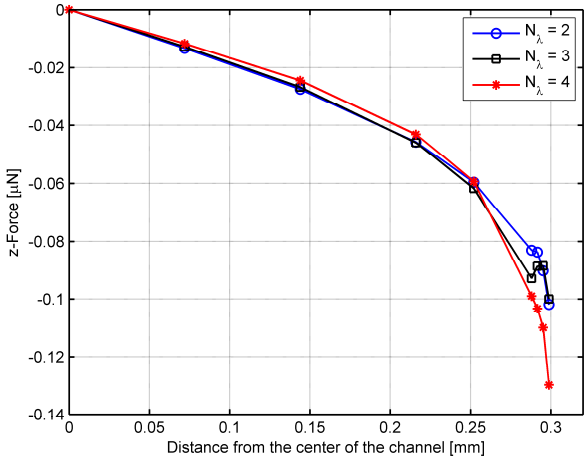

Figure 9. **z-**forces acting on the swimmers with respect to the distance from the center line of the channel for N_λ=2 (solid lines with circles), N_λ=3 (dashed line with circles), and N_λ=4 (dash-dotted line with '*'s).

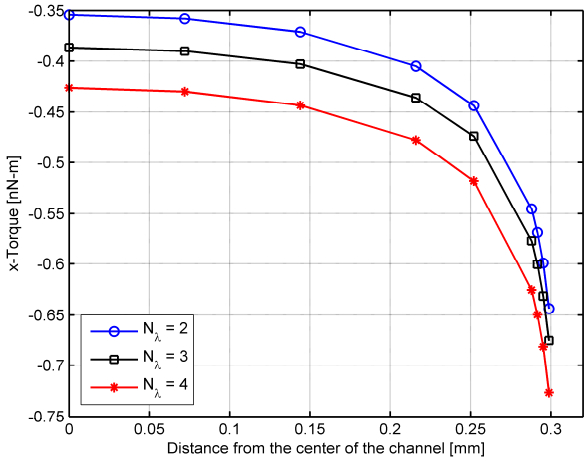

Figure 10. **x-**torques forces acting on the swimmers with respect to the distance from the center line of the channel for N_λ=2 (solid lines with circles), N_λ=3 (dashed line with circles), and N_λ=4 (dash-dotted line with '*'s).

Torque values are both negative and smaller in magnitude compared to **x**-torque in **y**- and **z-**directions. Non-zero values of **y-** and **z-**direction torques emphasize that the swimmer tends to change its initial alignment, which is parallel to the channel's long axis. As the number of waves on the helical tail decreases, the effect of **y-**direction torque increases. The difference between the cases of which number of waves equals three and four cannot be detected clearly. The sharp increase of the magnitudes of the **y-** and **z-**torques as micro swimmer approaches to the channel boundary can be seen in Fig. 11 and Fig. 12. Negative **y-** and **z-**torques indicate that micro robot has a tendency to change its alignment with respect to channels long axis in clock-wise directions with respect to **y-** and **z-**axis.

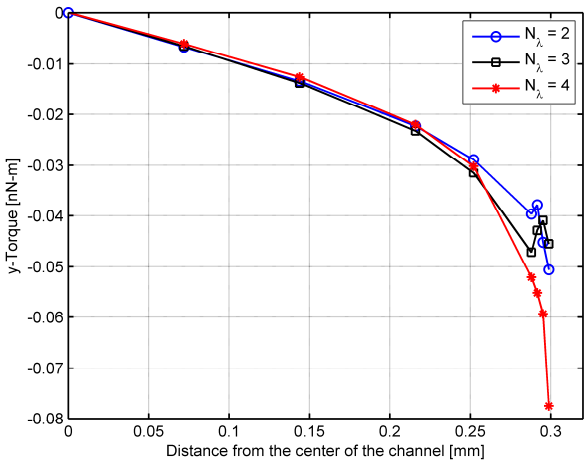

Figure 11. **y-**torques forces acting on the swimmers with respect to the distance from the center line of the channel for N_λ=2 (solid lines with circles), N_λ=3 (dashed line with circles), and N_λ=4 (dash-dotted line with '*'s).

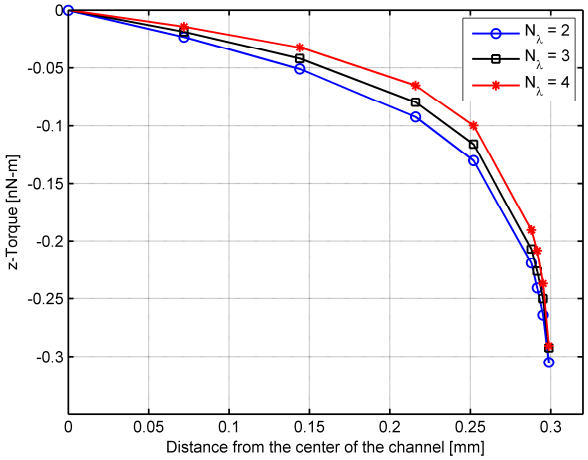

Figure 12. **z-**torques forces acting on the swimmers with respect to the distance from the center line of the channel for N_λ=2 (solid lines with circles), N_λ=3 (dashed line with circles), and N_λ=4 (dash-dotted line with '*'s).

IV. Conclusion

Experiments conducted with a micro robot that consists of a magnetic head and non-magnetic helical tail, show that the robots do not always move along the long-axis of the cylindrical channels. Micro robot's orientation and proximity to the channel boundaries affect its swimming speed. Computational fluid dynamics (CFD) simulations are conducted for the micro swimmer used in the experiments; results show that, as micro robot approaches to the channel wall, forward velocity increases. When compared to the experimental results for the case having the same Reynolds number, simulation results show that micro robot tends to travel near the wall when bounded with a cylindrical channel.

In accordance with simulation results, the place where micro robots travel fastest and most efficient is approximately 0.6-channel-radius away from the axis of the channel, a similar result for spherical objects in cylindrical channels is previously reported in [20]. Increase in magnitude of **y-** and **z-**

forces and **x-**, **y-**, and **z-**torques disturbs the in-parallel position and orientation of the swimmer with the channel axis as the swimmer is placed near the channel wall. Compared to the traction force, negative **z-**direction force is not as much dominant as to change the position of the micro robot. The positive traction force indicates that the micro robot has a tendency to trace the channel walls due to the friction between the robot and the wall. Increase in **x-**direction torque as the proximity to the channel wall increases leads to the need for higher intensity magnetic torques needed for synchronized rotation of the micro robot with the rotating magnetic field for near-wall swimming. The **z-**direction torque is more prominent compared to the **y-**direction torque, thus under the effect of the first one, micro swimmer orients itself towards its starboard direction. Moreover as the number of waves on the helical tail increases lower swimming speeds, higher traction forces and torques are observed.

Lastly, the radial position and the orientation of the micro robot inside the channel could not be detected precisely in our previous experiments. We aim to measure the three-dimensional motion of micro robot with the help of micro particle-image velocimetry techniques, which will help validating our CFD results as well as further understanding of the motion of micro swimming robots inside fluid-filled channels.

ACKNOWLEDGMENT

This work is supported by TUBITAK (Turkish Scientific and Technological Research Council of Turkey) under the grant number 111M376.

REFERENCES

[1] B. J. Nelson, I. K. Kaliakatsos, and J. J. Abbott, "Microrobots for minimally invasive medicine," *Annual Reviews of Biomedical* Engineering, 2010.

[2] R. Dreyfus, J. Baudry, M. L. Roper, M. Fermigier, H. A. Stone, and J. Bibette, "Microscopic artificial swimmers," *Nature*, vol. 437, no. 6, pp. 862-864, 2005.

[3] L. Zhang, J. J. Abbott, L. Dong, K. Peyer, B. E. Kratochvil, H. Zhang, C: Bergeles and B. J. Nelson, "Characterization of the swimming properties of artificial bacterial flagella," *Nano Letters*, vol. 9, no. 10, pp. 3663-3667, 2009.

[4] A. Ghosh and P. Fischer, "Controlled propulsion of artificial magnetic nanostructured propellers," *Nano Letters*, vol. 9, no. 6, 2009.

[5] T. Atsumi, Y. Maekawa, T. Yamada, I. Kawagishi, Y. Imae, and M. Homma, "Effect of viscosity on swimming by the lateral and polar flagella of vibrio alginolyticus," *Journal of Bacteriology*, vol.178, no.16, pp. 5024-5026, 1996.

[6] H. C. Berg, *Random Walks in Biology*. Princeton, NJ, USA: Princeton University Press, 1993.

[7] J. P. Armitage and R. M. Macnab, "Unidirectional, intermittent rotation of the flagellum of rhodobacter sphaeroides," *Journal of Bacteriology*, vol. 169, no. 2, pp. 514-518, 1987.

[8] J. Gray and G. Hancock, "The propulsion of sea-urchin spermatozoa," *Journal of Experimental Biology*, vol. 32, pp. 802-814, 1955.

[9] S. J. Lighthill, *Mathematical Biofluiddynamics.*Society for Industrial and Applied Mathematics, 1975.

[10] C. Brennen and H. Winet, "Fluid mechanics of propulsion by cilia and flagella," *Annual Review of Fluid Mechanics*, vol. 9. pp. 339-398, Jan. 1977.

[11] E. Lauga, "Continuous breakdown of Purcell's scallop theorem with inertia," *Physics of Fluids*, vol. 061703, no. 4., June 2007.

[12] D. F. Katz, J. R. Blake, and S. L. Paveri-Fontana, "On the movement of slender bodies near plane boundaries at low Reynolds number," *Journal of Fluid Mechanics*, vol. 72, pp. 529-540, 1975.

[13] B. U. Felderhof, "Swimming at low Reynolds number of a cylindrical body in a circular tube," *Physics of Fluids*, vol. 22, pp. 1136041-6, 2010.

[14] E. Lauga and T. R. Powers, "The hydrodynamics of swimming microorganisms," *Reports on Progress in Physics*, vol. 72, pp. 1-36, 2009.

[15] F. Z. Temel and S. Yesilyurt, "Magnetically actuated micro swimming of bio-inspired robots in mini channels," presented at the IEEE International Conference on Mechatronics, ICM2011, Istanbu, Turkey, April 13-15, 2011, Paper IF-007366.

[16] A. G. Erman and S. Yesilyurt, "Swimming of onboard-powered autonomous robots in viscous fluid filled channels," presented at the IEEE International Conference on Mechatronics, ICM2011, Istanbul, Turkey, April 13-15, 2011, Paper IF-007633.

[17] COMSOL AB, "Comsol multiphysics modelling guide," COMSOL, Tech. Rep. TR-0200 (420-46)-3, Nov. 1988.

[18] A. F. Tabak, F. Z. Temel, and S. Yesilyurt, "Comparison on experimental and numerical results for helical swimmers inside channels,1 presented at the IEEE/RSJ Int. Conf. on Intelligent Robots and Systems, IROS 2011, San Francisco, USA, Sept. 25-30 2011.

[19] D. Jiles, *Introduction to Magnetissm and Magnetic Materials,* 2nd ed. London, UK: Chapman & Hall, 1998.

[20] J. Happel and H. Brenner, *Low Reynolds number hydrodynamics:with special applications to particulate media,*, Springer, 1973.

[21] E. M. Purcell, "Life at low Reynolds number," *American Journal of Physics,*vol.45, no.1, pp. 3-11, 1976.